Elastic properties of moiré lattices in epitaxial two-dimensional materials

Alexandre Artaud, Nicolas Rougemaille, Sergio Vlaic, Vincent Renard, Nicolae Atodiresei, Johann Coraux

Letter | Editors' Suggestion

Elastic properties of moiré lattices in epitaxial two-dimensional materials

Alexandre Artaud,[1,2,3] Nicolas Rougemaille,[1] Sergio Vlaic,[4] Vincent T. Renard,[2] Nicolae Atodiresei,[5] and Johann Coraux[1,*]

[1]*Université Grenoble Alpes, CNRS, Institut NEEL, Grenoble INP, 38000 Grenoble, France*
[2]*Université Grenoble Alpes, CEA, Grenoble INP, IRIG, PHELIQS, 38000 Grenoble, France*
[3]*Department of Quantum Nanoscience, Kavli Institute of Nanoscience, Delft University of Technology, 2628 CJ Delft, the Netherlands*
[4]*Laboratoire de Physique et d'Étude des Matériaux, ESPCI Paris, PSL University, CNRS UMR8213, Sorbonne Universités, 75005 Paris, France*
[5]*Peter Grünberg Institute and Institute for Advanced Simulation, Forschungszentrum Jülich, Wilhelm-Johnen-Straße, 52428 Jülich, Germany*

(Received 21 February 2022; revised 8 July 2022; accepted 18 October 2022; published 4 November 2022)

Unlike conventional two-dimensional (2D) semiconductor superlattices, moiré patterns in 2D materials are flexible and their electronic, magnetic, optical, and mechanical properties depend on their topography. Within a continuous+atomistic theory treating 2D materials as crystalline elastic membranes, we abandon the flat-membrane scenario usually assumed for these materials and address out-of-plane deformations. We confront our predictions to experimental analyses on model systems, epitaxial graphene, and MoS_2 on metals and reveal that compression/expansion and bending energies stored in the membrane can compete with adhesion energy, leading to a subtle moiré wavelength selection and the formation of wrinkles.

DOI: 10.1103/PhysRevB.106.L201402

Introduction. Two-dimensional (2D) materials host height fluctuations called nanoripples and are therefore never perfectly flat, behaving as ultimately thin membranes [1]. A substrate generally suppresses the dynamics of these height fluctuations [2]. If crystalline, it stabilizes ordered arrays of *static* nanoripples. Their origin lies in the lateral periodic variation of the local atomic stacking [Fig. 1(a)], imposed by the lattice mismatch/misorientation of the two materials, and forming a so-called (quasi)coincidence superlattice, i.e., a moiré pattern [3–6].

Moirés are ubiquitous in epitaxial 2D materials, including graphene [7], *h*-BN [8], and MoS_2 [9]. They enrich their electronic properties [10,11] and promote the self-organization of nanoclusters [12,13], molecules [13,14], and isolated atoms [15–17], with foreseeable unique magnetic and catalytic properties. The mechanical properties are modified too, by phonon localization or phonon branch replicas [18–20], which should manifest in the thermal properties [2]. Rationalizing these properties requires the knowledge of the wavelength Λ and amplitude Δ of the nanoripple pattern [Fig. 1(a)]. Λ is often simply evaluated geometrically, from the superposition of the individual 2D material and substrate lattices. Δ is often considered to be set by the strength of the interaction with the substrate [21–24] or a planar stress [25].

Here we investigate, numerically and experimentally, how Λ and Δ are interlinked through the *elasticity* of the 2D membrane. Introducing a mixed continuum mechanics/atomistic modeling we address the usually disregarded effects of non-planar deformations, i.e., bending, on nanorippling under the influence of a crystalline surface. This allows one to study moiré systems with numbers of atoms beyond what density functional theory (DFT) and molecular dynamics calculations can tackle, as shown previously for twisted bilayers [26,27]. We apply our model to two epitaxial 2D materials. Comparing graphene on Ir with and without an intercalated Co monolayer, we investigate the influence of two substrates with the same lattice parameter but different binding strength. Furthermore, we demonstrate the generality of our method with another 2D material, MoS_2/Au. Separating the contributions to the total energy, we relate weak nanorippling to a form of the membrane-substrate interaction varying moderately across the moiré, which generates only small bending energy penalty provided that Λ is large enough (graphene/Ir, MoS_2/Au). A more subtle Λ selection is unveiled when the substrate promotes strong nanorippling (graphene/Co/Ir): the membrane mitigates its bending energy by increasing its planar-projected area. This is accommodated by local wrinkling, as confirmed by microscopy data.

Modeling. We apply elastic thin plate theory to a membrane having a sinusoidal topography, while taking into account the atomic arrangement at the substrate surface and within the membrane. Two vector fields are considered: the displacement field $\vec{u}$ associated with the membrane deformation and the geometrical phase $\vec{\varphi} \in [0, 2\pi]^2$ describing the coincidence between the membrane and substrate atoms [Fig. 1(a)]. The continuum mechanics and atomistic viewpoints are entangled in $\vec{u}$, which is at the same time a continuous $\vec{u}(x, y)$ and a discrete $\vec{u}_i$ field (defined for each atom i of the membrane). For simplicity, we assume a uniform interatomic distance d within the membrane and an infinite rigidity of the substrate lattice.

The membrane surface has the form $\Delta/9 \sum_{i=1}^{3} \cos(\vec{k}_i \cdot \vec{r}) + \Delta/3$ (graphene) and $\Delta/(3\sqrt{3}) \sum_{i=1}^{3} \sin(\vec{k}_i \cdot \vec{r}) + \Delta/2$

*johann.coraux@neel.cnrs.fr

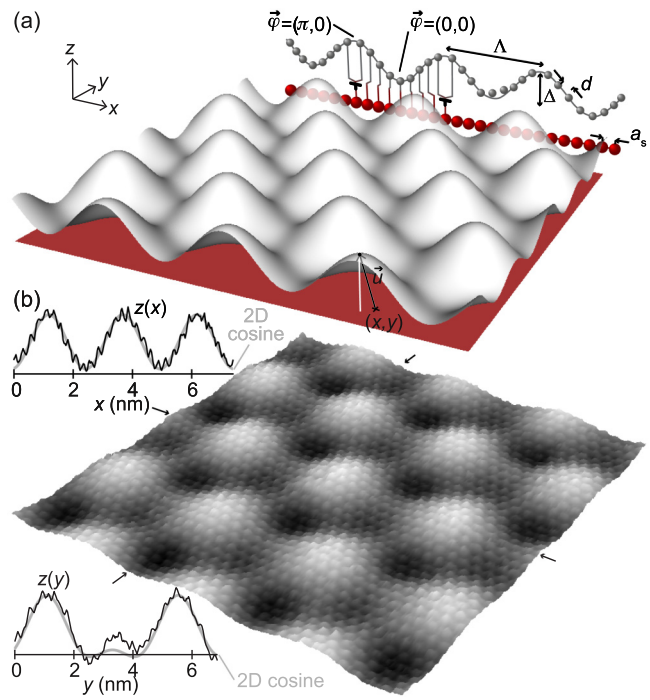

FIG. 1. (a) Points on the membrane are displaced from their position on a flat unrippled membrane by $\vec{u}(x, y)$. The cross section (top right) shows the moiré pattern's undulation (period Λ, amplitude Δ) and the atomic lattices (interatomic distances d and a_s in the membrane and substrate, respectively). The 2D phase $\vec{\varphi}$, i.e., the atomic stacking, varies from a valley to a hill. There, a substrate atom stands halfway between two membrane atoms ($\top$ symbols). (b) STM topograph (8×8 nm^2) of a graphene membrane onto Ir(111) and apparent height profiles extracted between the arrows fitted using a cosine function.

(MoS_2) [28], with $\vec{r}$ a 2D position vector and $\vec{k}_{i=1,2,3}$ three $2\pi/3$-rotated vectors of norm $4\pi/(\Lambda\sqrt{3})$. The elastic energy $E_{\rm el} = 1/2 \int \mathrm{Tr}\,(\varepsilon\sigma)dx\,dy = \int e_{\rm el} dx\,dy$ is decomposed, using the stress-strain (σ and ε tensors) relationship and the Lamé coefficients (λ, μ), bending rigidity (κ), and Poisson ratio (ν) [29], in in-plane (ip) and out-of-plane (oop) components [30]:

$$\begin{aligned} E_{\rm el,ip} =& \frac{1}{2}\int \big[\lambda(\varepsilon_{xx}+\varepsilon_{yy})^2 \\ &+ 2\mu\big(\varepsilon_{xx}^2+\varepsilon_{yy}^2+2\varepsilon_{xy}^2\big)\big]dx\,dy, \\ E_{\rm el,oop} =& \frac{\kappa}{2}\int \{(\partial_x\partial_x u_z+\partial_y\partial_y u_z)^2+2(1-\nu) \\ &\times[(\partial_x\partial_y u_z)^2-\partial_x\partial_x u_z\partial_y\partial_y u_z]\}dx\,dy, \end{aligned} \tag{1}$$

with $\varepsilon_{\alpha\beta} = 1/2(\partial_\beta u_\alpha + \partial_\alpha u_\beta + \sum_{\tau=x,y,z}\partial_\alpha u_\tau \partial_\beta u_\tau)$, $\alpha, \beta = x, y$, and $\partial_{\alpha,\beta} = \partial/\partial_{\alpha,\beta}$.

The adhesion energy of the membrane on the substrate is written as a sum over the atomic positions:

$$E_{\rm ad} = \sum_i e_{{\rm ad},i}(\vec{\varphi}_i, u_{z,i}). \tag{2}$$

The elastic and adhesion energies are functions of Λ, Δ, the relative orientation θ of the membrane and substrate lattices (Sec. S1.7 of the Supplemental Material [39]), and d [40]. Calculating $E_{\rm ad}$ requires knowledge of the $e_{{\rm ad},i}$ potential, which depends on the kind of substrate and the local membrane-substrate atomic coincidence. For epitaxial 2D materials, $e_{{\rm ad},i}$ has at least one minimum, for heights of the 2D material that change within the moiré cell (with i). This promotes nanorippling and hence an $e_{\rm el}$ penalty (unless d is compressed) that tends to mitigate it. We search for the lowest-energy structure of the membrane, among the set of $E_{\rm el} + E_{\rm ad}$ values calculated over a unit cell of the nanoripple pattern, for an extended range of $\{d, \Lambda, \Delta\}$ triplets. We also assessed the influence of θ.

For each system, 6000 triplets were used, varying d within $\pm 1\%$ around graphene's or MoS_2's reference values (2.462 Å, 3.167 Å; Sec. S1.2 of the Supplemental Material [39]), Λ across 20–30 Å or 28–38 Å (graphene, MoS_2), and Δ across 0.05–2.4 Å—by steps of 0.25%, 0.2 Å, and 0.1 Å, respectively. Based on DFT calculations, including our own new ones for MoS_2/Au(111), accounting for van der Waals interactions at the membrane/substrate interface, we parametrized the adhesion potentials. The elastic constants were taken from the relevant calculations and experimental estimates (Secs. S1.1, S1.3, and S1.4 of the Supplemental Material [39]). The minimum-energy configurations were then compared to our scanning tunneling microscopy (STM) measurements (Sec. S2 of the Supplemental Material [39]) and other previously published experimental data.

Weak nanorippling. High-resolution measurement of Λ, Δ, and d is notoriously challenging experimentally. Graphene on Ir(111) is one of the few systems for which this has been done [21,25,31–34] and MoS_2/Au(111) another one, albeit to a lesser extent [36–38]. The measured structural parameters are reported in Table I—Δ estimates vary with the tunneling imaging conditions for graphene/Ir [33], even more so for MoS_2/Au [37]. A typical STM topograph of graphene/Ir(111) is shown in Fig. 1(b). Apparent height profiles through the moiré pattern, along high-symmetry directions, are well described by the 2D cosine function introduced above [Fig. 1(b)].

A Morse potential faithfully describes the adhesion energy, $e_{{\rm Ir\text{-}C},i}$, in particular the presence of a large-distance energy minimum (>3 Å). This minimum only slightly varies with the local atomic coincidence; it is much related to a van der Waals interaction that prevails at weak-interaction interfaces between graphene and metals like Cu, Ag, Ir, Pt, and Au [41,42]. The potential has been parametrized to obtain an average binding energy per C atom close to the 50 meV value derived from DFT calculations (Sec. S1.3 of the Supplemental Material [39]). Computing the elastic energy requires knowledge on the elastic constants λ, μ, and ν, which have been estimated for graphene/Ir(111) [43], whereas κ is only known for graphite [44] (Sec. S1.1 of the Supplemental Material [39]).

The calculated minimum-energy d and Δ (Table I) fit within the range of experimental values [21,33,34], whereas Λ is slightly larger (we will come back to that). Interestingly, the elastic energy marginally contributes to the total energy. Considering the adhesion energy alone leads to similar estimates of Λ and Δ [noted Λ' and Δ' in Table I, Figs. S6(b,c) of the Supplemental Material [39]]. The

TABLE I. Calculated elastic $\bar{e}_{\rm el}$ and adhesion $\bar{e}_{\rm ad}$ contributions to the total energy $\bar{e}_{\rm t}$, normalized by the number of atoms (meV/Å^2), in a moiré unit cell, for optimal values of d variation (%), Λ (Å), and Δ (Å). $\Lambda = \Lambda'$ and $\Delta = \Delta'$ values minimize $\bar{e}_{\rm ad}$ alone. Experimental structural parameters from the literature and our STM measurements (*) are reported.

	Δd	Λ	Δ	$\bar{e}_{\rm ad}$	$\bar{e}_{\rm el}$	$\bar{e}_{\rm t}$	Λ'	Δ'
Graphene/Ir	−0.05	26.4	0.39	−11.94	0.04	−11.90	26.4	0.43
Experiments	−0.01/−0.29 [31]	25.5, 25.6 [31,32], 25.4*	0.6/1.0, 0.42/0.56, 0.38 [21,33,34], 0.35*					
Graphene/Co/Ir	+0.17	27.3	1.67	−12.56	0.85	−11.71	25.3	2.03
Experiments	+0.1/1.4 [35]	26.5/28.5 [35]	1.2/1.8 [23], 1.8*					
MoS_2/Au	−0.25	35.2	0.44	−30.74	0.23	−30.50	32.8	0.46
Experiments	−0.32, +0.13 [36,37]	33.4, 33.3 [37,38]	0.37 [37]					

topography is essentially inherited from the C-Ir interaction (Λ and Δ Table I) and graphene/Ir(111) is a weakly nanorippled system storing little elastic energy. This holds too for graphene slightly twisted (fractions of degrees are often observed experimentally [33,45]) with respect to Ir(111) (Sec. S1.7 of the Supplemental Material [39]).

As the elastic energy reflects the membrane curvature, it is inhomogeneous in space, with $E_{\rm el,oop}$ [Eq. (1)] as its main contribution. It is maximum at the top of the nanoripples [dark regions in Fig. 2(a)], minimum along their flanks (white regions), and takes intermediate values at the surface's saddle points and valleys (orange regions).

The spatial distribution of the adhesion energy is simpler [Figs. 2(a) and 2(c)]: it follows the surface topography, with the weakest (strongest) binding at the hills (valleys). This reflects the varying graphene-on-Ir stacking configuration, with half the C atoms located on top of the Ir ones (valleys) and the center of C hexagons on top of Ir atoms (hills) [21].

For MoS_2/Au, we calculate three times stronger adhesion energy and six times stronger elastic energy than for graphene/Ir (Table I). Their spatial distribution is also well explained by the varying local stacking and membrane bending (Fig. S5 of the Supplemental Material [39]). Although it is more costly to bend MoS_2 than graphene, the energy penalty still appears affordable, presumably owing to the large Λ value.

Strong bending effects. To gain insight on the influence of adhesion on nanorippling we now consider graphene on Ir with Co intercalated (Sec. S2 of the Supplemental Material [39]). The Co surface is pseudomorphic to Ir (same lattice constant) but has a different kind of adhesion. Compared to graphene/Ir, a five-to-ten-fold increase of Δ is found in STM, depending on the tunnel bias voltage [Figs. 2(a) and 2(b)] [23,46].

In the discussion above, the adhesion energy $e_{{\rm Ir},i}$ had a single minimum, at a (large) distance varying only slightly with the atomic coincidence, which promoted weak nanorippling. According to *ab initio* calculations [41,42], surfaces having high affinity with C, especially Co and Ni, lead to the occurrence of a second minimum at shorter distance (∼2.2 Å) for coincidences with half C atoms atop a metal atom (Figs. S1,S3, Sec. S1.3 of the Supplemental Material [39]). Adhesion energy variations are in the same range as for $e_{{\rm Ir},i}$, but the large distance between the two

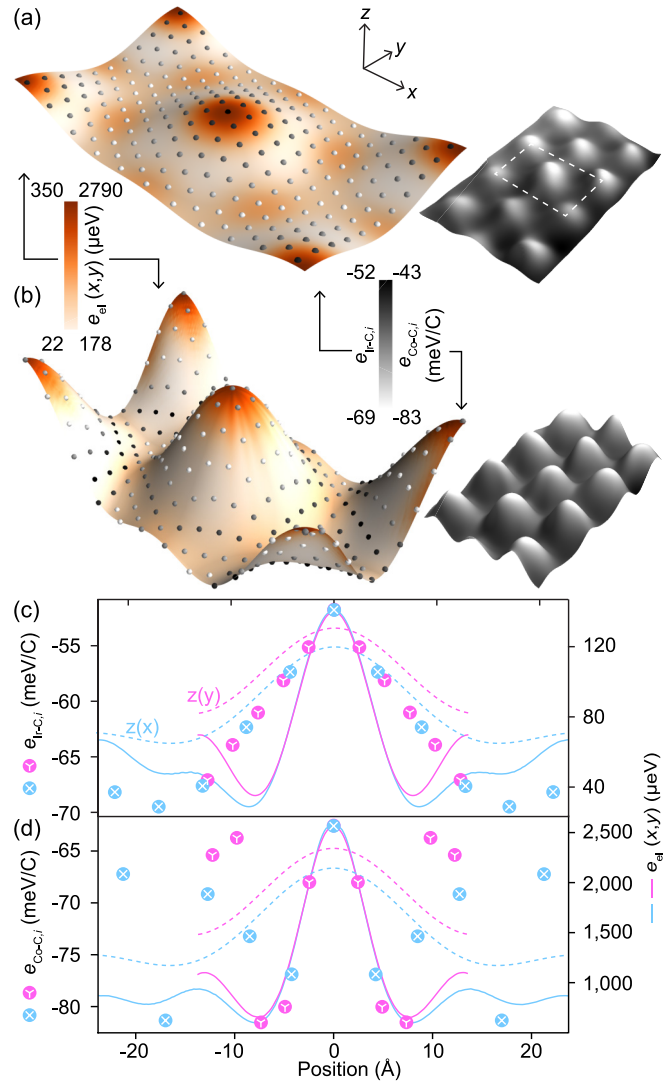

FIG. 2. (a),(b) Spatial distribution of the elastic ($e_{\rm el}$ evaluated on a square grid with 0.2 Å steps) and adhesion ($e_{{\rm Ir\text{-}C},i}$, $e_{{\rm Co\text{-}C},i}$) energy densities for graphene on Ir and Co/Ir, and corresponding STM topographs (9 × 6.5 nm^2; one unit cell sketched with a dotted frame). The z scale is multiplied by 10. (c),(d) Cross sections, along x and y axes, of the membrane's height (dotted lines) and corresponding elastic (solid lines) and adhesion (X and Y symbols) energies, for graphene/Ir (c) and graphene/Co/Ir (d).

minima promotes strong nanorippling. Our analytical form of $e_{\mathrm{Co},i}$ adds a Gaussian component to the Morse potential to account for the two minima.

The $\{d, \Lambda, \Delta\}$ triplet minimizing the system energy yields a four times larger Δ value than for graphene/Ir and agrees well with the experimental estimates (Table I, Refs. [23,46]). Λ is also substantially larger in the presence of the intercalated Co layer (which is pseudomorphic to Ir). Our calculations show [Fig. S7(b) of the Supplemental Material [39]] that this results from the six-times stronger out-of-plane (bending) energy density here. Note the larger (by about 0.2%) interatomic distance d, now significantly off the reference value. The corresponding in-plane (stretching) elastic energy penalty, more than ten times that in graphene/Ir, is compensated by a gain in adhesion energy, allowed by the larger d that yields favorable substrate-membrane atomic coincidences (while the opposite effect is associated with the increased rippling). These behaviors are also found for small twist angles of the graphene lattice (Sec. S1.7 of the Supplemental Material [39]).

As expected, the spatial distribution of the elastic energy density is essentially the same as for graphene/Ir [Figs. 2(b) and 2(d)], with most of the energy being stored at high curvature regions, i.e., the hills, the valleys, and the saddle points. The spatial distribution of the adhesion energy density is more complex here. In particular, the valleys of the membrane are no longer the only regions with strong adhesion energy and the spatial variations are much faster [Figs. 2(c) and 2(d)]. Changing the metal substrate thus deeply modifies the adhesion energy density within the membrane.

Mechanical instability. Our calculations predict Λ values larger by $\sim$1 Å and $\sim$2 Å, respectively, than experimental values for graphene/Ir [31,32] and MoS_2/Au [37,38] (Table I). Such discrepancies are expected as a result of the heteroepitaxial stress building up as the samples are cooled down after growth, due to the mismatch in thermal expansion coefficients of the 2D material and the substrate. In graphene/Ir this stress is only partially relieved to the expense of a local bending and loss of adhesion, by linear delaminations called wrinkles [32]; no wrinkles form to relieve the (smaller) stress in MoS_2/Au [36]. In other words, experimentally graphene/Ir and MoS_2/Au are close but not exactly at the calculated equilibrium state. For their lower Λ values, we calculate lower estimates of the excess total energy, compared to the equilibrium state, of only 4 meV (graphene/Ir) and 2 meV (MoS_2/Au) per unit cell. This is because the total energy weakly depends on Λ when $\Delta \simeq 0.4$ Å [Fig. S6(c) of the Supplemental Material [39]]. If thermodynamic equilibrium is not precisely reached experimentally (growth is an out-of-equilibrium process), the total energy is only weakly affected.

This is not the case with graphene/Co/Ir, for which this energy difference is, depending on the graphene twist angle ($0°$, $0.5°$, $1°$), 20 to 60 times larger due to strong elastic energy variations at large Δ values [Fig. S6(d) of the Supplemental Material [39]]. As discussed above this is the driving force for a complex Δ and Λ selection, beyond what the adhesion energy alone would impose. This large excess bending energy, in graphene/Co/Ir with $\Delta \simeq 25.5$ Å, may be relieved by an increase of Λ and hence an increase of the projected

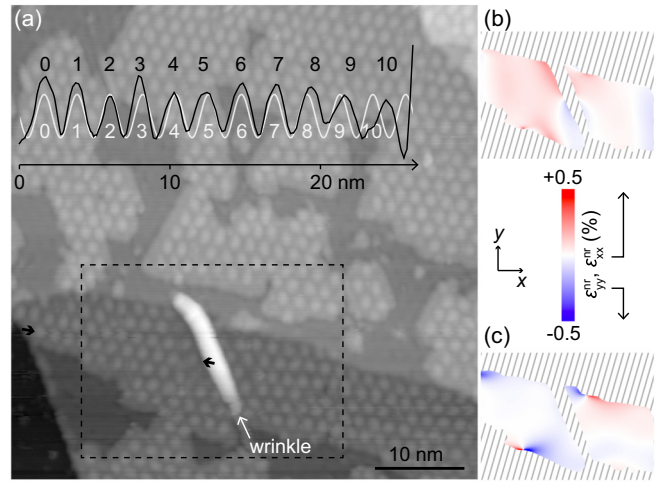

FIG. 3. (a) STM topograph of graphene/Ir intercalated with a Co submonolayer. A graphene wrinkle appears as a bright linear feature. Inset: apparent height profile between the two black arrows, compared to a sinusoid (the successive maxima are numbered). (b),(c) Maps of the moiré lattice compression/expansion in the xy plane, roughly perpendicular (c) and parallel (d) to the wrinkle.

membrane's area. The latter must be accommodated somewhere. This is what experiments reveal: a second network of wrinkles forms upon Co intercalation. This new network is easily recognized: wrinkles are lower, shorter, and denser than those formed after graphene growth (Fig. S8 of the Supplemental Material [39]).

One wrinkle in this new network, at an intermediate stage of the intercalation process, is visible in Fig. 3(a). We analyzed the in-plane deformations $\varepsilon_{xx}^{\mathrm{nr}}$ and $\varepsilon_{yy}^{\mathrm{nr}}$ in the x and y directions of the nanoripple (nr) lattice at the vicinity of the wrinkle using a geometrical phase analysis (Sec. S3 of the Supplemental Material [39]). A gradient of $\varepsilon_{xx}^{\mathrm{nr}}$ is observed perpendicular to the wrinkle [Fig. 3(b)]: the nanoripple lattice is stretched when approaching the wrinkle. In fact, the moiré lattice expands by several tenths of a percent, bringing Λ to values close to, and even at, those we predict for the lowest-energy configuration (Table I). Consistently, in (apparent) height profiles, Λ increases as the distance to the wrinkle shortens [Fig. 3(a)]. On the contrary, in the direction parallel to the wrinkle there is no obvious $\varepsilon_{yy}^{\mathrm{nr}}$ variation close to the wrinkle [Fig. 3(c)]. Other effects seem to play a more important role in this direction—for instance, the presence of a substrate step edge or the edge of the intercalated Co island.

Altogether, our spatially resolved analysis of the deformation field in the nanoripple pattern supports the above proposal for a wrinkling mechanism induced by an "unrippling" (Λ increase) of the membrane. This mechanism highlights the far-reaching consequences of the mechanical (elastic) backaction of the membrane under the influence of a substrate.

Prospects. Our model predicts the ground-state structure of graphene and MoS_2 on substrates with different adhesion properties. Experimental data are close to these predictions, with only minor discrepancies that vanish if bending energy penalties matter, i.e., for strongly rippled systems. We identify

where and how the 2D membrane stores energy *via* elastic deformations, bending in particular, and disentangle the role of the substrate from that of the membrane's mechanical properties. Altogether these are of utmost importance to understanding and engineering nanorippling-related properties, e.g., pseudoelectromagnetic fields, excitonics, and electronic correlations [47]. Our approach is complementary to first-principle ones, permitting fast calculations (<1 s) on large systems and the exploration of a broad range of parameters (Λ, a_s, θ). It is also applicable to twisted 2D bilayers in the presence of strain fields [26,27]—altogether, to help interpret the rich moiré-related phenomena, including disorder [31,33,48,49] and temperature effects.

Acknowledgments. We thank P. David and V. Guisset for valuable support with the ultrahigh vacuum experiments and J.-L. Rouvière for providing a geometrical phase analysis software. N.A. acknowledges Deutsche Forschungsgemeinschaft (DFG) support through the Collaborative Research Center SFB 1238 Project No. 277146847 (subproject C01). The authors gratefully acknowledge the computing time granted by the JARA Vergabegremium and provided on the JARA Partition part of the supercomputer JURECA at Forschungszentrum Jülich. V.T.R. acknowledges the support from ANR Flatmoi project (No. ANR-21-CE30-0029). We thank A. Locatelli, T. O. Menteş, and B. Santos for assistance during the low-energy electron microscopy measurements.

[1] A. Fasolino, J. Los, and M. I. Katsnelson, Intrinsic ripples in graphene, Nat. Mater. **6**, 858 (2007); J. C. Meyer, A. K. Geim, M. I. Katsnelson, K. S. Novoselov, T. J. Booth, and S. Roth, The structure of suspended graphene sheets, Nature (London) **446**, 60 (2007); J. Brivio, D. T. Alexander, and A. Kis, Ripples and layers in ultrathin MoS_2 membranes, Nano Lett. **11**, 5148 (2011).

[2] B. Amorim and F. Guinea, Flexural mode of graphene on a substrate, Phys. Rev. B **88**, 115418 (2013).

[3] K. Hermann, Periodic overlayers and moiré patterns: theoretical studies of geometric properties, J. Phys.: Condens. Matter **24**, 314210 (2012).

[4] A. Artaud, L. Magaud, T. Le Quang, V. Guisset, P. David, C. Chapelier, and J. Coraux, Universal classification of twisted, strained and sheared graphene moiré superlattices, Sci. Rep. **6**, 25670 (2016).

[5] P. Zeller and S. Günther, What are the possible moiré patterns of graphene on hexagonally packed surfaces? universal solution for hexagonal coincidence lattices, derived by a geometric construction, New J. Phys. **16**, 083028 (2014).

[6] P. Pochet, B. C. McGuigan, J. Coraux, and H. T. Johnson, Toward moiré engineering in 2d materials via dislocation theory, Appl. Mater. Today **9**, 240 (2017).

[7] T. Land, T. Michely, R. Behm, J. Hemminger, and G. Comsa, Stm investigation of single layer graphite structures produced on Pt(111) by hydrocarbon decomposition, Surf. Sci. **264**, 261 (1992).

[8] M. Corso, W. Auwärter, M. Muntwiler, A. Tamai, T. Greber, and J. Osterwalder, Boron nitride nanomesh, Science **303**, 217 (2004).

[9] S. G. Sørensen, H. G. Füchtbauer, A. K. Tuxen, A. S. Walton, and J. V. Lauritsen, Structure and electronic properties of in situ synthesized single-layer MoS_2 on a gold surface, ACS Nano **8**, 6788 (2014).

[10] I. Pletikosić, M. Kralj, P. Pervan, R. Brako, J. Coraux, A. T. N'Diaye, C. Busse, and T. Michely, Dirac Cones and Minigaps for Graphene on Ir(111), Phys. Rev. Lett. **102**, 056808 (2009).

[11] M. Papagno, D. Pacilé, D. Topwal, P. Moras, P. M. Sheverdyaeva, F. D. Natterer, A. Lehnert, S. Rusponi, Q. Dubout, F. Calleja, E. Frantzeskakis, S. Pons, J. Fujii, I. Vobornik, M. Grioni, C. Carbone, and H. Brune, Two distinct phases of bilayer graphene films on Ru'(0001), ACS Nano **6**, 9299 (2012).

[12] A. T. N'Diaye, S. Bleikamp, P. J. Feibelman, and T. Michely, Two-Dimensional Ir Cluster Lattice on a Graphene Moiré on Ir(111), Phys. Rev. Lett. **97**, 215501 (2006).

[13] H. Dil, J. Lobo-Checa, R. Laskowski, P. Blaha, S. Berner, J. Osterwalder, and T. Greber, Surface trapping of atoms and molecules with dipole rings, Science **319**, 1824 (2008).

[14] J. Mao, H. Zhang, Y. Jiang, Y. Pan, M. Gao, W. Xiao, and H.-J. Gao, Tunability of supramolecular kagome lattices of magnetic phthalocyanines using graphene-based moiré patterns as templates, J. Am. Chem. Soc. **131**, 14136 (2009).

[15] R. Balog, B. Jørgensen, L. Nilsson, M. Andersen, E. Rienks, M. Bianchi, M. Fanetti, E. Lægsgaard, A. Baraldi, S. Lizzit, Z. Sljivancanin, F. Besenbacher, B. Hammer, T. G. Pedersen, P. Hofmann, and Hornekær, Bandgap opening in graphene induced by patterned hydrogen adsorption, Nat. Mater. **9**, 315 (2010).

[16] R. Baltic, M. Pivetta, F. Donati, C. Wäckerlin, A. Singha, J. Dreiser, S. Rusponi, and H. Brune, Superlattice of single atom magnets on graphene, Nano Lett. **16**, 7610 (2016).

[17] S. Trishin, C. Lotze, N. Bogdanoff, F. von Oppen, and K. J. Franke, Moiré Tuning of Spin Excitations: Individual Fe Atoms on MoS_2/Au(111), Phys. Rev. Lett. **127**, 236801 (2021).

[18] M. Endlich, H. P. Miranda, A. Molina-Sánchez, L. Wirtz, and J. Kröger, Moiré-induced replica of graphene phonons on Ir(111), Ann. Phys. (NY) **526**, 372 (2014).

[19] D. Maccariello, A. Al Taleb, F. Calleja, A. Vázquez de Parga, P. Perna, J. Camarero, E. Gnecco, D. Farías, and R. Miranda, Observation of localized vibrational modes of graphene nanodomes by inelastic atom scattering, Nano Lett. **16**, 2 (2016).

[20] A. Al Taleb, G. Anemone, D. Farías, and R. Miranda, Resolving localized phonon modes on graphene/Ir(111) by inelastic atom scattering, Carbon **133**, 31 (2018).

[21] C. Busse, P. Lazić, R. Djemour, J. Coraux, T. Gerber, N. Atodiresei, V. Caciuc, R. Brako, A. T. N'Diaye, S. Blügel, J. Zegenhagen, and T. Michely, Graphene on Ir(111): Physisorption with Chemical Modulation, Phys. Rev. Lett. **107**, 036101 (2011).

[22] B. Wang, M.-L. Bocquet, S. Marchini, S. Günther, and J. Wintterlin, Chemical origin of a graphene moiré overlayer on Ru(0001), Phys. Chem. Chem. Phys. **10**, 3530 (2008).

[23] R. Decker, J. Brede, N. Atodiresei, V. Caciuc, S. Blügel, and R. Wiesendanger, Atomic-scale magnetism of cobalt-intercalated graphene, Phys. Rev. B **87**, 041403(R) (2013).

[24] P. Sutter, J. T. Sadowski, and E. A. Sutter, Chemistry under cover: tuning metal-graphene interaction by reactive intercalation, J. Am. Chem. Soc. **132**, 8175 (2010).

[25] S. Runte, P. Lazić, C. Vo-Van, J. Coraux, J. Zegenhagen, and C. Busse, Graphene buckles under stress: An x-ray standing wave and scanning tunneling microscopy study, Phys. Rev. B **89**, 155427 (2014).

[26] N. N. T. Nam and M. Koshino, Lattice relaxation and energy band modulation in twisted bilayer graphene, Phys. Rev. B **96**, 075311 (2017).

[27] V. V. Enaldiev, V. Zólyomi, C. Yelgel, S. J. Magorrian, and V. I. Fal'ko, Stacking Domains and Dislocation Networks in Marginally Twisted Bilayers of Transition Metal Dichalcogenides, Phys. Rev. Lett. **124**, 206101 (2020).

[28] The atomic structure of graphene and MoS_2 are different, which yields qualitatively different kinds of 2D variations of the adhesion potential with the substrate (see Sec. S1.2 of the Supplemental Material [39]) and hence qualitatively different topographies.

[29] L. Landau and E. Lifschitz, *Course of Theoretical Physics, Theory of Elasticity Vol. 7* (Pergamon Press, London, 1959).

[30] Note that u_z is not simply the height on membrane surface, but the z coordinate of the elementary surface element on the membrane, displaced by the deformation of the latter [Fig. 1(a)].

[31] N. Blanc, J. Coraux, C. Vo-Van, A. T. N'Diaye, O. Geaymond, and G. Renaud, Local deformations and incommensurability of high-quality epitaxial graphene on a weakly interacting transition metal, Phys. Rev. B **86**, 235439 (2012).

[32] H. Hattab, A. T. N'Diaye, D. Wall, C. Klein, G. Jnawali, J. Coraux, C. Busse, R. van Gastel, B. Poelsema, T. Michely, F.-J. Meyer zu Heringdorf, and M. Horn-von Hoegen, Interplay of wrinkles, strain, and lattice parameter in graphene on iridium, Nano Lett. **12**, 678 (2012).

[33] S. K. Hämäläinen, M. P. Boneschanscher, P. H. Jacobse, I. Swart, K. Pussi, W. Moritz, J. Lahtinen, P. Liljeroth, and J. Sainio, Structure and local variations of the graphene moiré on Ir(111), Phys. Rev. B **88**, 201406(R) (2013).

[34] F. Jean, T. Zhou, N. Blanc, R. Felici, J. Coraux, and G. Renaud, Effect of preparation on the commensurabilities and thermal expansion of graphene on Ir(111) between 10 and 1300 K, Phys. Rev. B **88**, 165406 (2013).

[35] P. Gargiani, R. Cuadrado, H. B. Vasili, M. Pruneda, and M. Valvidares, Graphene-based synthetic antiferromagnets and ferrimagnets, Nat. Commun. **8**, 699 (2017).

[36] H. Bana, E. Travaglia, L. Bignardi, P. Lacovig, C. E. Sanders, M. Dendzik, M. Michiardi, M. Bianchi, D. Lizzit, F. Presel, D. De Angelis, N. Apostol, P. K. Das, H. Fujii, I. Vobornik, R. Larciprete, A. Baraldi, P. Hofmann, and S. Lizzit, Epitaxial growth of single-orientation high-quality MoS_2 monolayers, 2D Mater. **5**, 035012 (2018).

[37] C. C. Silva, D. Dombrowski, N. Atodiresei, W. Jolie, F. Farwick zum Hagen, J. Cai, P. T. P. Ryan, P. K. Thakur, V. Caciuc, S. Blügel, D. A. Duncan, T. Michely, T.-L. Lee, and C. Busse, Spatial variation of geometry, binding, and electronic properties in the moiré superstructure of MoS_2 on Au(111), 2D Mater. **9**, 025003 (2022).

[38] R. Sant, S. Lisi, V. D. Nguyen, E. Mazaleyrat, A. C. Gómez Herrero, O. Geaymond, V. Guisset, P. David, A. Marty, M. Jamet, C. Chapelier, L. Magaud, Y. J. Dappe, M. Bianchi, P. Hofmann, G. Renaud, and J. Coraux, Decoupling molybdenum disulfide from its substrate by cesium intercalation, J. Phys. Chem. C **124**, 12397 (2020).

[39] See Supplemental Material at http://link.aps.org/supplemental/10.1103/PhysRevB.106.L201402 for details about the simulation methods, elastic constants, additional simulation data, and sample preparation and characterization (see, also, Refs. [50–70] therein).

[40] The latter dependency is explicit for E_{ad} and implicit for E_{el}, corresponding to a change of the total membrane surface when d deviates from the reference unstrained value.

[41] T. Olsen and K. S. Thygesen, Random phase approximation applied to solids, molecules, and graphene-metal interfaces: From van der Waals to covalent bonding, Phys. Rev. B **87**, 075111 (2013).

[42] M. S. Christian, A. Otero-De-La-Roza, and E. R. Johnson, Adsorption of graphene to metal (111) surfaces using the exchange-hole dipole moment model, Carbon **124**, 531 (2017).

[43] A. Politano and G. Chiarello, Probing the Young's modulus and Poisson's ratio in graphene/metal interfaces and graphite: a comparative study, Nano Res. **8**, 1847 (2015).

[44] R. Nicklow, N. Wakabayashi, and H. Smith, Lattice dynamics of pyrolytic graphite, Phys. Rev. B **5**, 4951 (1972).

[45] A. T. N'Diaye, J. Coraux, T. N. Plasa, C. Busse, and T. Michely, Structure of epitaxial graphene on Ir(111), New J. Phys. **10**, 043033 (2008).

[46] D. Pacilé, S. Lisi, I. Di Bernardo, M. Papagno, L. Ferrari, M. Pisarra, M. Caputo, S. K. Mahatha, P. M. Sheverdyaeva, P. Moras, P. Lacovig, S. Lizzit, A. Baraldi, M. G. Betti, and C. Carbone, Electronic structure of graphene/Co interfaces, Phys. Rev. B **90**, 195446 (2014).

[47] Z. Dai, L. Liu, and Z. Zhang, Strain engineering of 2D materials: issues and opportunities at the interface, Adv. Mater. **31**, 1805417 (2019).

[48] H. Ochoa, Moiré-pattern fluctuations and electron-phason coupling in twisted bilayer graphene, Phys. Rev. B **100**, 155426 (2019).

[49] M. Koshino and Y.-W. Son, Moiré phonons in twisted bilayer graphene, Phys. Rev. B **100**, 075416 (2019).

[50] J.-W. Jiang, Z. Qi, H. S. Park, and T. Rabczuk, Elastic bending modulus of single-layer molybdenum disulfide (MoS_2): finite thickness effect, Nanotechnology **24**, 435705 (2013).

[51] R. C. Cooper, C. Lee, C. A. Marianetti, X. Wei, J. Hone, and J. W. Kysar, Nonlinear elastic behavior of two-dimensional molybdenum disulfide, Phys. Rev. B **87**, 035423 (2013).

[52] K. Zakharchenko, M. Katsnelson, and A. Fasolino, Finite Temperature Lattice Properties of Graphene beyond the Quasiharmonic Approximation, Phys. Rev. Lett. **102**, 046808 (2009).

[53] E. Dwight, *American Institute of Physics Handbook Vol. 1* (McGraw-Hill, New York, 1972).

[54] S. El-Mahalawy and B. Evans, The thermal expansion of 2H-MoS_2, 2H-$MoSe_2$ and 2H-WSe_2 between 20 and 800°C, J. Appl. Crystallogr. **9**, 403 (1976).

[55] D. Stradi, S. Barja, C. Díaz, M. Garnica, B. Borca, J. Hinarejos, D. Sánchez-Portal, M. Alcamí, A. Arnau, A. V. De Parga, R. Miranda, and F. Martín, Role of Dispersion Forces in the Structure of Graphene Monolayers on Ru Surfaces, Phys. Rev. Lett. **106**, 186102 (2011).

[56] F. Mittendorfer, A. Garhofer, J. Redinger, J. Klimeš, J. Harl, and G. Kresse, Graphene on Ni (111): Strong interaction and weak adsorption, Phys. Rev. B **84**, 201401 (2011).

[57] D. Newns, Self-consistent model of hydrogen chemisorption, Phys. Rev. **178**, 1123 (1969).

[58] P. Hohenberg and W. Kohn, Inhomogeneous electron gas, Phys. Rev. **136**, B864 (1964).

[59] P. E. Blöchl, Projector augmented-wave method, Phys. Rev. B **50**, 17953 (1994).

[60] G. Kresse and J. Hafner, *Ab initio* molecular dynamics for liquid metals, Phys. Rev. B **47**, 558 (1993).

[61] G. Kresse and J. Furthmüller, Efficient iterative schemes for *ab initio* total-energy calculations using a plane-wave basis set, Phys. Rev. B **54**, 11169 (1996).

[62] W. Kohn and L. J. Sham, Self-consistent equations including exchange and correlation effects, Phys. Rev. **140**, A1133 (1965).

[63] K. Lee, É. D. Murray, L. Kong, B. I. Lundqvist, and D. C. Langreth, Higher-accuracy van der Waals density functional, Phys. Rev. B **82**, 081101 (2010).

[64] A. Becke, On the large-gradient behavior of the density functional exchange energy, J. Chem. Phys. **85**, 7184 (1986).

[65] J. P. Perdew, K. Burke, and M. Ernzerhof, Generalized Gradient Approximation Made Simple, Phys. Rev. Lett. **77**, 3865 (1996).

[66] I. Hamada, van der Waals density functional made accurate, Phys. Rev. B **89**, 121103 (2014).

[67] T. Menteş, G. Zamborlini, A. Sala, and A. Locatelli, Cathode lens spectromicroscopy: methodology and applications, Beilstein J. Nanotechnol. **5**, 1873 (2014).

[68] M. Takeda and J. Suzuki, Crystallographic heterodyne phase detection for highly sensitive lattice-distortion measurements, J. Opt. Soc. Am. A **13**, 1495 (1996).

[69] M. Hÿtch, E. Snoeck, and R. Kilaas, Quantitative measurement of displacement and strain fields from HREM micrographs, Ultramicroscopy **74**, 131 (1998).

[70] J.-L. Rouviere and E. Sarigiannidou, Theoretical discussions on the geometrical phase analysis, Ultramicroscopy **106**, 1 (2005).